COMMUNICATION

A Metal-Oxide Interconnection Layer for Polymer Tandem Solar Cells with an Inverted Architecture

*Cheng-Hsuan Chou, Wei Lek Kwan, Ziruo Hong, Li-Min Chen, and Yang Yang**

In the past decade, polymer solar cells have attracted considerable interest due to their potential for low-cost, light-weight and flexible applications.[1,2] As a result of efficient exciton dissociation in polymer-fullerene blends, polymer bulk heterojunction (BHJ) solar cells with high external quantum efficiencies (EQE, ratio of extracted charge carriers to incident photons) can be achieved by carefully controlling the morphology of the polymer blend.[3,4] The power conversion efficiency (PCE) can be further improved by using low band gap polymers which absorb a broader range of photon energies that also provide a better match to the solar spectrum.[5–7] However, the ultimate achievable efficiency of the solar cell is still limited by the low carrier mobility and narrow absorption spectra of the polymers.[8] Low mobility of the polymer material constrains the active layer thickness because a thicker film will lower the extraction efficiency of charge carriers, while a thinner film will lead to insufficient absorption of incident photons. The limited absorption spectrum of the polymer also results in inefficient utilization of the solar spectrum. To overcome these challenges, it is desirable to stack individual cells with complementary absorption in a tandem structure to realize high efficiency polymer tandem cells.[9–13] Typical polymer tandem cells consist of two diodes, head-to-tail connected via an interlayer. Conductive polymers, e.g., poly(3,4-ethylenedioxythiophene) blended with poly(styrenesulfonate) (PEDOT:PSS), and n-type metal oxides are commonly used as the interlayer. However, the acidic nature of PEDOT:PSS raises stability concerns.[14] In addition, optical loss due to absorption of the PEDOT:PSS film is significant, approaching 10% in the visible range, and even higher in the near infrared (NIR) region.[15] Metal oxides with higher stability and optical transparency has thus been proposed to replace PEDOT:PSS as the interfacial layer between indium tin oxide (ITO) and polymer BHJs. Furthermore, the polarity of the solar cells can be controlled by the properties of the metal oxides.[16,17] Devices with an inverted architecture, where the positions of the anode and cathode are reversed, have been demonstrated with better stability. This is because the reactive low work function metal in a regular configuration is replaced by an inorganic electron collection layer, including Cs_2CO_3,[17,18] TiO_2,[19,20] TiO_2:Cs_2CO_3,[21] or ZnO.[22–24] The counter electrode is composed of a relatively stable hole collection layer covered by a high work function metal. The absence of PEDOT:PSS and low work function metals indicates promising long term stability of the inverted structure.

Despite recent advancements in polymer solar cells with the tandem and inverted architectures, reports on high efficiency polymer tandem cell utilizing the inverted configuration remain scarce. The challenge lies in designing and realizing the optimal combination of both the polymer materials and the interlayer. While complementary absorption of the tandem structure meets this optical requirement, the interlayer inserted between the two sub-cells should be not only robust enough to protect the underlying layers against subsequent solvents, but also provide an effective electrical contact. Fundamentally, the interlayer works as a metal wire bringing together the electron quasi-Fermi level of one sub-cell to the hole quasi-Fermi level of the other, adding up the potential of the two polymer BHJs. Therefore, an interlayer simultaneously satisfying the optical and electrical properties is a prerequisite for high efficiency polymer tandem cells. Resistance against solvents in solution processes is yet another challenge for metal oxides as the interlayer, according to the obvious open circuit voltage (V_{oc}) loss when using MoO_3 as the anode buffer layer.[26]

In this manuscript, we explore the configuration of tandem polymer solar cells with the inverted structure, employing a metal oxide-only interlayer to connect two polymer BHJs with the benefits of complementary absorption and potentially improved stability. Good electrical and optical coupling of the two sub-cells is achieved by using a carefully-designed MoO_3/Al/ZnO layer, which leads to a PCE of 5.1% in our inverted tandem solar cell. Compared to PEDOT:PSS, the absorption of the metal oxide-based interlayer is negligible throughout the visible to NIR spectral range, resulting in high photocurrent for both single and tandem cells. Our results demonstrated that effective connection between polymer BHJs can be realized by this simple oxide interlayer. As a result, the materials and configurations of the interlayer are no longer limited by the acidic PEDOT:PSS.

The device structure of the optimized inverted polymer tandem solar cell is shown in **Figure 1a**. Two polymers with complementary absorption spectra are selected for the active layers. Starting from the transparent cathode side, i.e., indium tin oxide (ITO)/ZnO, the bottom sub-cell is based on a poly(3-hexylthiophene) (P3HT): [6,6]-phenyl C_{61} butyric acid methyl ester ($PC_{60}BM$) layer. As for the top sub-cell, a low band gap polymer poly[(4,4′-bis(2-ethylhexyl)dithieno[3,2-b:2′,3′-d] silole)-2,6-diyl-alt-(2,1,3-benzothiadiazole)-4,7-diyl] (PSBTBT)

C.-H. Chou, W. L. Kwan, Dr. Z. R. Hong, L.-M. Chen, Prof. Y. Yang
Department of Materials Science and Engineering
University of California
Los Angeles, CA 90095, USA
E-mail: yangy@ucla.edu
C.-H. Chou
Phosphors Research Laboratory
Department of Applied Chemistry
National Chiao Tung University
Hsinchu 30050, Taiwan, Republic of China

DOI: 10.1002/adma.201001033

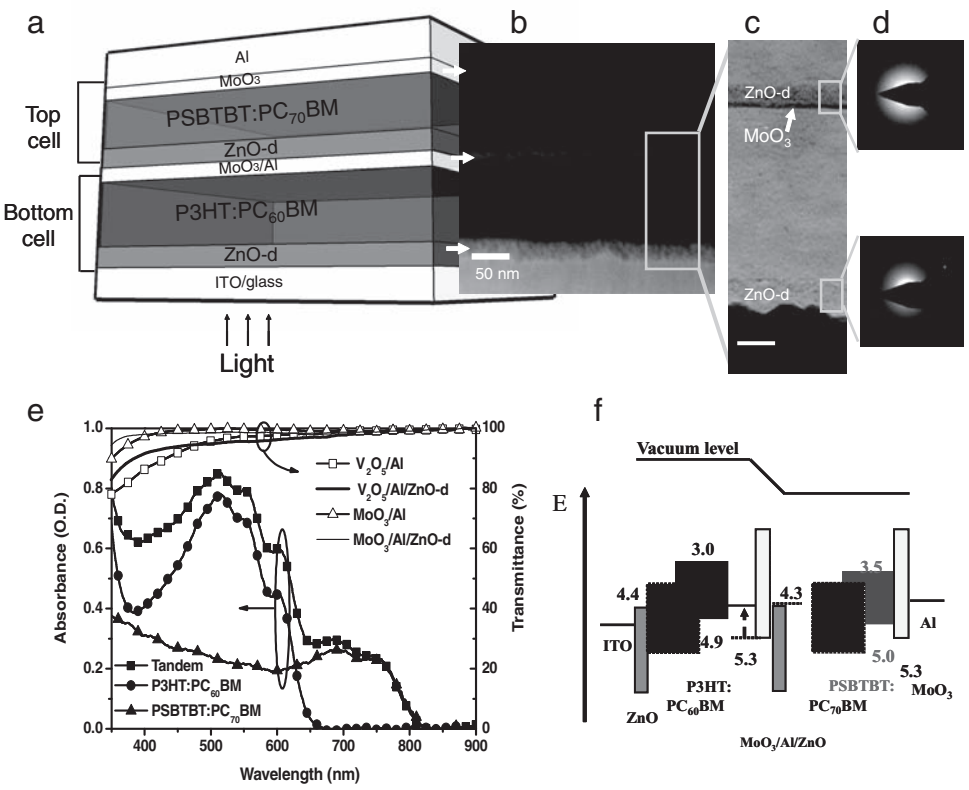

Figure 1. a) The device structure, b) cross-sectional SEM image, c) TEM image (right) of the inverted polymer tandem solar cell and d) TEM diffraction of ZnO-d films. e) Absorption spectra of reference BHJ films and the tandem cell prior to cathode deposition, and the transmittance spectra of the interlayers with and without the ZnO-d film. f) Energy-level diagram of the tandem cell.

blended with $PC_{70}BM$ is used.[6] The optimal thicknesses of the bottom and top sub-cells are 150 and 120 nm, respectively. The connecting metal-oxide interlayer consists of MoO_3 (10 nm by thermal evaporation) and ZnO (30 nm by sol-gel process) for effective hole and electron collection, respectively. An aluminum layer (1 nm by thermal evaporation) is inserted between MoO_3 and ZnO to provide excellent electrical contacts and good processability, which its role will be discussed later. Cross-sectional scanning electron microscopy (SEM) and transmission electron microscopy (TEM) images in Figure 1b,c show well-defined individual layers. The absorption spectra of the optimized tandem cell, as well as the P3HT:$PC_{60}BM$ and PSBTBT:$PC_{70}BM$ blends, are shown in Figure 1e. The absorption of P3HT:$PC_{60}BM$ film spans from 400 to 630 nm, which mainly corresponds to the π–π* transition of P3HT and a minor contribution from $PC_{60}BM$. The low band gap PSBTBT:$PC_{70}BM$ film shows a relatively flat absorption curve throughout the visible range from the combined absorption of the polymer in the NIR range and the $PC_{70}BM$ in the visible range. The overall absorption of the stacked polymer BHJs, together with the MoO_3/Al/ZnO interlayer, exceeds 0.8 optical density (O.D.) from 350–600 nm, and reaches 0.3 O.D. at 750 nm. Figure 1e also compares the transmittance (T%) of these metal oxides with 1 nm-thick Al layer (V_2O_5/Al and MoO_3/Al) before and after the ZnO film deposition. The high T% exceeding 95% of MoO_3/Al/ZnO film and similar V_2O_5-based interlayer ensures minimal optical loss in the UV-visible-NIR region. Considering the transmittance and work function, MoO_3 was chosen as the anode buffer layer for both subcells for hole extraction. Consequently, the MoO_3/Al/ZnO transparent interlayer was constructed as the interconnecting layer in the tandem structure to facilitate charge recombination between the bottom and top sub-cells.

Figure 1f illustrates the energy level diagram of the tandem cell structure, indicating the highest occupied molecular orbital (HOMO) energies and the lowest unoccupied molecular orbital (LUMO) energies of each component, as well as the work functions of the conductive electrodes. ZnO on ITO forms a low work function cathode contact for the bottom sub-cell, while MoO_3 (work function ~5.3 eV) delivers an efficient anode contact.[25] Similarly, the top sub-cell also starts from ZnO, with a top anode contact composed of MoO_3/Al.

The performances of the tandem and reference single cells are characterized under simulated AM 1.5G solar illumination of 100 mW cm^{-2} as shown in **Figure 2a**. The P3HT:$PC_{60}BM$ single cell yields a PCE of 3.2%, with open-circuit voltage (V_{oc}) of 0.58 V, short-circuit current (J_{sc}) of 8.6 mA cm^{-2}, and fill factor (FF) of 64%. The low band gap PSBTBT:$PC_{70}BM$ reference cell exhibits a PCE of 3.7%, with V_{oc} = 0.64 V, J_{sc} = 11.7 mA cm^{-2}, and FF = 49%. The inverted configuration has been well established for P3HT:PCBM system, here we further explore that relatively high PCE can also be obtained from other polymers. The large difference in J_{sc} from the reference cells was compensated by placing the P3HT:$PC_{60}BM$ BHJ in the front as the bottom sub-cell. The tandem cell yields a PCE of 5.1%, with

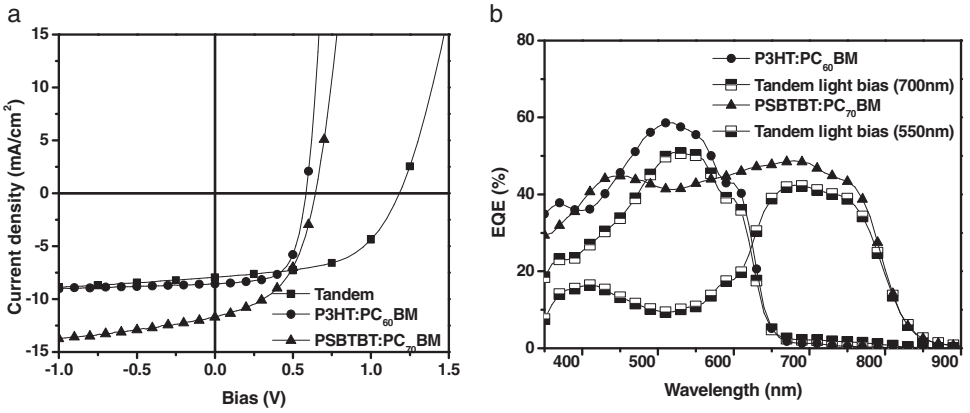

Figure 2. a) *J–V* characteristics of the reference single (ITO/ZnO-d/photoactive polymer:fullerene blend/MoO_3/Al), and tandem cells using MoO_3/Al/ZnO as the interlayer between the two sub-cells, measured under simulated AM1.5G, 100 mW cm^{-2} illumination. b) EQE of sub-cells in the tandem structure (with monocolor light bias) and respective reference single cells.

V_{oc} = 1.20 V, J_{sc} = 7.8 mA cm^{-2}, and FF = 54%. From the view point of electrical connection, the Voc of the tandem cell is equal to the sum of the two sub-cells, confirming the efficient coupling of the two sub-cells in series, in which the quasi-Fermi level alignment between MoO_3 and ZnO results in a significant vacuum level shift. The J_{sc} from the inverted tandem cell is slightly higher than the reported value from regular structure based on PEDOT:PSS as the anode buffer layer.[13] We believe this is due to the high T% of the metal oxide layers, resulting in minimal optical loss. The EQE measurement for each sub-cell and reference single cells was performed,[12] and the results are shown in Figure 2b. The P3HT:PC_{60}BM cell exhibits EQE maximum at 500 nm, whilst the EQE of the PSBTBT:PCBM cell is approximately around 45% from 400 to 800 nm. When incorporated into the tandem architecture, we employ monochromatic light to selectively turn on one of the sub-cells to conduct accurate EQE measurements for the other. The EQE of the P3HT:PCBM bottom cell decreases to ~50% at 500 nm, while the PSBTBT:PCBM top sub-cell significantly drops from 350 to 650 nm, mainly due to the spectral overlap. The *J–V* characteristics and the EQE results confirm that the interlayer provides an optimal coupling between the two sub-cells with minimal optical or electrical losses.

The interlayer engineering needs to take into account several factors. An effective interlayer should possess the following properties: (1) high transmittance; (2) good electrical contact for both sub-cells; (3) impermeability to protect against solvents. For the interlayer consisting of metal oxides, a compatible deposition technique is also of essential importance. New processing issues arise for the inverted tandem cells since the interlayer deposition sequence is reversed. ZnO was chosen as the electron collection layer for both the bottom and top sub-cells based on its stability and processability. For sol-gel processed ZnO using zinc acetate as the precursor, temperature as high as 300 °C is needed to complete the thermal decomposition of the zinc acetate and even higher temperature is required to form crystalline ZnO (abbreviated ZnO-c).[24] In order to avoid the high temperature process, which is detrimental to the underlying polymer, low temperature process at 150 °C for hydrolysis of the ZnO layers was developed. At this temperature, the evaporated solvent (2-methoxyethanol) leaves behind zinc acetate residue in the resultant ZnO film (abbreviated ZnO-d).[27] To test the

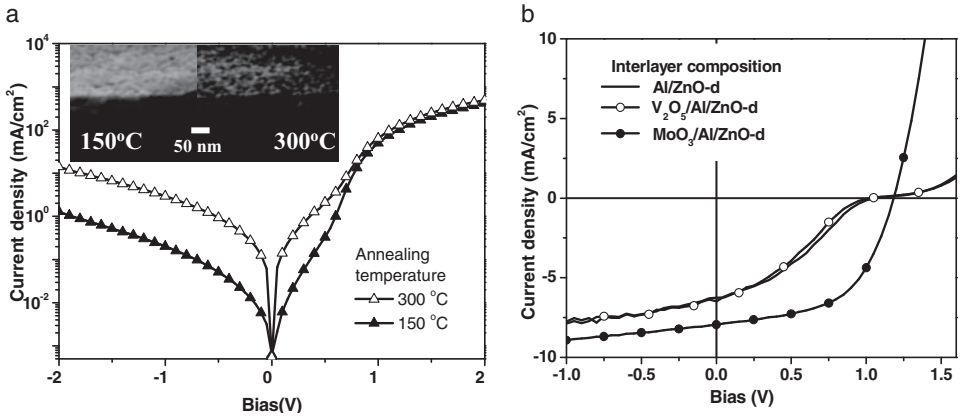

Figure 3. a) Dark *J–V* curves of the single cells with amorphous ZnO-d layer (solid triangle) and crystalline ZnO-c layer (triangle) devices. Insert: SEM images of ZnO on ITO with annealing temperature at 150 °C and 300 °C, respectively. b) *J–V* characteristics of tandem cells with different interlayer combination, I: Al/ZnO-d, II: V_2O_5/Al/ZnO-d, III: MoO_3/Al/ZnO-d, under simulated AM1.5G solar illumination of 100 mW cm^{-2}.

feasibility of the ZnO-d film as the electron collection layer in the inverted structure, P3HT:PC_{60}BM cells on two types of ZnO films were fabricated. According to the dark *J–V* characteristics shown in **Figure 3a**, the ZnO-d device exhibited excellent diode characteristics with higher rectification ratio and lower leakage current under reverse bias than the device based on the ZnO-c film. To further identify the origin of the leakage current, microscopic studies were carried out. The SEM images in the inset of Figure 3a reveal a dense and smooth ZnO-d film. On the contrary, the ZnO-c film appears relatively porous and rough, where the voids are likely formed during $Zn(OAc)_2$ decomposition.[24,27] The TEM diffraction pattern in Figure 1d implies that the ZnO-d film has an amorphous structure, although no difference in the series resistance (Rs) was observed from the *J–V* characteristics. This indicates that ZnO-d has excellent electron transporting properties despite its amorphous nature. Unfortunately, electrical properties such as the carrier density and conductivity of the amorphous ZnO-d layer were difficult to characterize quantitatively and further evaluation of the interlayer is undergoing. The instability of ZnO under ultrahigh vacuum hinders reliable characterization of the work functions via ultra-violet photoelectron spectroscopy (UPS). However, possible work function differences aside, the smooth surface and dense structure of the ZnO-d film suppress hole injection from the ITO side under reverse bias, leading to a high FF of 64% in the single cell. Furthermore, in the tandem architecture, the ZnO-d film is effective in blocking solvent penetration upon subsequent polymer active layer deposition, and its processing temperature is compatible with polymer BHJs, which is extremely critical for the interlayer connecting two sub-cells in the tandem structure. The dense ZnO-d films are helpful to achieve V_{oc} add-up in tandem cells. Gilot et al. proposed that the V_{oc} of the tandem cells is usually lower than the V_{oc} summation of single reference cells due to the counterdiode behavior of the p-n junction connecting the two sub-cells.[9] However, this counterdiode effect can be avoided with proper materials combination. Our findings indicate that low temperature processed-ZnO-d films function not only as an efficient n-type contact layer for polymer BHJs, but also as an effective electrical connection in tandem structures.

The compatibility of ZnO-d with hole-collecting metal oxides in the interlayer was also studied. Tandem devices with three types of interlayers, namely Al/ZnO-d, V_2O_5/Al/ZnO-d and MoO_3/Al/ZnO-d were fabricated. The ultrathin Al layer serves as a wetting layer for the ZnO deposition, as well as forming ohmic contacts and providing additional recombination sites.[28,29] The *J–V* curves and detailed photovoltaic performance of the tandem cells implementing interlayers of various metal oxides are shown in Figure 3b and summarized in **Table 1**, respectively. The device utilizing MoO_3 delivered excellent photovoltaic behavior, while the other two devices exhibit much inferior performance. The lower photocurrent can be ascribed to poor charge selectivity of the interlayer, while the s-shape *J–V* behavior near V_{oc} indicates a significant energy barrier for charge extraction and injection.[30,31] For Al/ZnO-d, incomplete coverage of the ultrathin aluminum layer is incapable of separating the P3HT:PCBM BHJ from the ZnO-d film in the interlayer. In this case, the P3HT:PCBM film simultaneously contacts with both the top and bottom ZnO films, which reduces the build-in potential of the bottom sub-cell. Consequently, the electrons may flow out of the BHJ film from both sides, and reduces the photocurrent as shown in Figure 3b. The poor charge selectivity of the interlayer also induces significant electron accumulation in the ZnO layer due to the overwhelming electrons from both the bottom and top BHJs. The unbalanced charge injection into the interlayer results in the s-shape behavior and a substantially lower V_{oc} of 1.05 V, as well as larger Rs. Interestingly, the tandem cell based on a V_2O_5/Al/ZnO-d interlayer also shows a similar S-shape behavior. This is due to the fact that V_2O_5 is an amphoteric oxide that reacts with both strong non-reducing acids and alkali. It is thus dissolved in the ZnO precursor solution that produces acetic acid during the sol-gel process. Electrons are drained out through direct contact of the bottom BHJ with the ZnO layer, which is consistent with a low shunt resistance (R_{sh}) of the two tandem cells without MoO_3 shown in Table 1. In contrast, MoO_3 is acidic in nature and dissolves in water over neutral to alkaline pH range and is more robust against the ZnO sol-gel process.[32] Therefore, the MoO_3-based interlayer retains its hole collection capability even after the ZnO process. Due to the above issues, it is shown that the processability of the interlayer is crucial to construct efficient tandem solar cells.

Table 1. Photovoltaic performance of tandem cells with three interlayer structures.

Interlayer	V_{oc} (V)	J_{sc} (mA/cm^2)	PCE (%)	FF (%)	R_p (Ω cm^2)	R_s (Ω cm^2)
Al/ZnO	1.05	6.55	2.0	28.7	3546.2	19.7
V_2O_5/Al/ZnO	1.05	6.47	2.0	29.0	1053.5	17.0
MoO_3/Al/ZnO	1.20	7.84	5.1	54.1	6857.3	2.27

In conclusion, we have successfully demonstrated a highly efficient inverted polymer tandem solar cell. A highly transparent, low temperature processable amorphous ZnO-d layer with excellent charge selectivity is introduced, which is the foundation in achieving the high PCE in our inverted devices. Physical and chemical compatibility of the metal oxide systems for electrical connectivity, i.e., charge collection and recombination, were also studied. Effective electrical and optical coupling of the two sub-cells are achieved by using the carefully designed MoO_3/Al/ZnO-d layer. The proposed interlayer structures, as well as the materials selection and processing, could be applied to various polymer materials and open opportunities for multi-stacked inverted tandem solar cells.

Experimental Section

The device architecture of the inverted tandem cell is shown in Figure 1a. The tandem cells were fabricated on ITO-coated glass substrates, with sheet resistance of 15Ω/□. The pre-cleaned ITO substrates were treated with UV-ozone prior to the spin-coating of the ZnO-d precursor solution consisting of 0.5 M zinc acetate dihydrate in 0.5 M monoethanolamine and 2-methoxyethanol at 4000 r.p.m. for 40 s, followed by baking at 150 °C for 5 min in ambient air. The ZnO-d films were then rinsed in de-ionized water, acetone, and isopropyl alcohol and then dried to remove organic residues from the surface, and transferred to a nitrogen-filled glove box for polymer deposition. The first active layer was deposited by spin-coating P3HT:P_{60}CBM blend films by the solvent annealing method[1] from a 1:1 wt. ratio solution in 1,2-dichlorobenzene (15 mg of P3HT in 1 mL of solvent) at 600 r.p.m.

The films were then annealed at 110 °C for 10 min. 10 nm MoO_3 and 1 nm Al were subsequently thermally evaporated on top of the bottom cell. An amorphous ZnO-d layer was deposited with a precursor solution consisting of 0.3 M zinc acetate and 0.3 M monoethanolamine in 2-methoxyethanol at a spin speed of 4000 rpm for 40 s). The film was annealed at 150 °C for 5 min in ambient air. The second active layer was spin-coated at 4500 r.p.m. for 30 s from PSBTBT:$PC_{70}BM$ (1:1) in chloroform (10 mg of PSBTBT/ 1 mL of solvent) and thermally annealed at 150 °C for 5 min. Finally, to complete the solar cell device, 10 nm of MoO_3 and 70 nm of aluminum as the anode were thermally evaporated through a shadow mask. The device area, as defined by the overlap between the ITO and Al electrodes, was 0.093 $cm^{2.}$ The absorption and transmittance data was taken using a Varian Cary 50 Ultraviolet-Visible Spectrophotometer. All the electrical measurements were performed in a nitrogen-filled glove box at room temperature. Current-Voltage characteristics of the tandem cell both in the dark and under light were taken using a Kiethley 2400 source unit. Light *I–V* curves were taken under 100 mW cm^{-2} simulated AM1.5G illumination from an Oriel 9600 solar simulator. EQE spectra were measured by using a lock-in amplifier (SR830, Stanford Research Systems) under short circuit condition while the devices were illuminated by a monochromatic light from a xenon lamp passing through a monochromator (SpectraPro-2150i, Acton Research Corporation). To measure EQE of individual sub-cells in the tandem structure, monochromatic light at 500 and 700 nm are used to excite the bottom P3HT and top PSBTBT sub-cells, respectively.

Acknowledgements

C.-H.C. and W.L.K. contributed equally to this work. The authors would like to thank Dr. Srinivas Sista, Dr. Judy Park, Mr. Bao Lei for technical discussions, Dr. Lijun Huo and Dr. Jianhui Hou for supplying the PSBTBT polymer, Dr. Sergey Prikhodko and Ms. Biyun Li for TEM imaging, and Mr. Eric Richards for proofreading the manuscript. Prof. Yang would like to thank Prof. Yongfang Li of Chinese Academic of Science for technical discussion. The financial support is from the Air Force Office of Scientific Research (AFOSR, grant # FA95500710264), National Science Foundation (grant #CHE0822573). L.-M. Chen acknowledges financial support from NSF IGERT: Materials Creation Training Program (MCTP) (DGE-0114443) and California NanoSystems Institute. C.-H. Chou would like to thank the National Science Council of Taiwan, Project NSC-0962917-I-009–112 for financial support.

Received: March 22, 2010
Published online: September 9, 2010

[1] K. M. Coakley, M. D. McGehee, *Chem. Mater.* **2004**, *16*, 4533.
[2] C. J. Brabec, N. S. Sariciftci, J. C. Hummelen, *Adv. Funct. Mater.* **2001**, *11*, 15.
[3] G. Li, V. Shrotriya, J. Huang, Y. Yao, T. Moriarty, K. Emery, Y. Yang, *Nat. Mater.* **2005**, *4*, 864.
[4] W. Ma, C. Y. Yang, X. Gong, K. Lee, A. J. Heeger, *Adv. Funct. Mater.* **2005**, 15, 1617.
[5] J. Peet, J. Y. Kim, N. E. Coates, W. L. Ma, D. Moses, A. J. Heeger, G. C. Bazan, *Nat. Mater.* **2007**, *6*, 497.
[6] J. H. Hou, H.-Y. Chen, S. Q. Zhang, G. Li, Y. Yang, *J. Am. Chem. Soc.* **2008**, *130*, 16144.
[7] Y. Liang, D. Feng, Y. Wu, S. T. Tsai, G. Li, C. Ray, L. Yu, *J. Am. Chem. Soc.*, **2009**, *131*, 7792.
[8] A. Hadipour, B. de Boer, J. Wildeman, F. B. Kooistra, J. C. Hummelen, M. G. R. Turbiez, M. M. Wienk, R. A. J. Janssen, P. W. M. Blom, *Adv. Funct. Mater.* **2006**, *16*, 1897.
[9] J. Gilot, M. M. Wienk, R. A. J. Janssen, *Appl. Phys. Lett.* **2007**, *90*, 143512.
[10] T. Ameri, G. Dennler, C. Lungenschmied, C. J. Brabec, *Energy Environ. Sci.* **2009**, *2*, 347.
[11] A. Hadipour, B. de Boer, P. W. Blom, *Adv. Funct. Mater.* **2008**, *18*, 169.
[12] J. Y. Kim, K. Lee, N. E. Coates, D. Moses, T.-Q. Nguyen, M. Dante, A. J. Heeger, *Science* **2007**, *317*, 222.
[13] S. Sista, M. H. Park, Z. Hong, Y. Wu, J. Hou, W. L. Kwan, G. Li, Y. Yang, *Adv. Mater.* **2010**, *22*, 380.
[14] M. P. de Jong, L. J. van IJzendoorn, M. J. A. de Voigt, *Appl. Phys. Lett.* **2000**, *77*, 2255.
[15] S. C. J. Meskers, J. K. J. van Duan. R. A. J. Janssen, *Adv. Funct. Mater.* **2003**, *13*, 805.
[16] Y. Sahin, S. Alem, R. Bettignies, J.-M. Nunzi, *Thin Solid Films*, **2005**, *476*, 340.
[17] G. Li, C. W. Chu, V. Shrotriya, J. Huang, Y. Yang, *Appl. Phys. Lett.* **2006**, *88*, 253503.
[18] H.-H. Liao, L.-M. Chen, Z. Xu, G. Li, Y. Yang, *Appl. Phys. Lett.* **2008**, *92*, 173303.
[19] G. K. Mor, K. Shankar, M. Paulose, O. K. Varghese, C. A. Grimes, *Appl. Phys. Lett.* **2007**, *91*, 152111.
[20] M. S. White, D. C. Olson, S. E. Shaheen, N. Kopidakis, D. S. Ginley, *Appl. Phys. Lett.* **2006**, *89*, 143517.
[21] M.-H. Park, J.-H. Li, A. Kumar, G. Li, Y. Yang, *Adv. Funct. Mater.* **2009**, *19*, 1241.
[22] C. Waldauf, M. Morana, P. Denk, P. Schilinsky, K. Coakley, S. A. Choulis, C. J. Brabec, *Appl. Phys. Lett.* **2006**, *89*, 233517.
[23] S. K. Hau, H. L. Yip, N. S. Baek, J. Zou, K. O'Malley, A. K. Y. Jen, *Appl. Phys. Lett.* **2008**, *92*, 253301.
[24] N. Sekine, C.-H. Chou, W. L Kwan, Y. Yang. *Org. Electron.* **2009**, *10*, 1473.
[25] V. Shrotriya, G. Li, Y. Yao, C. W. Chu, Y. Yang, *Appl. Phys. Lett.* **2006**, *88*, 073508.
[26] D. W. Zhao, X. W. Sun, C. Y. Jiang, A. K. K. Kyaw, G. Q. Lo, D. L. Kwong, *IEEE Electron. Dev. Lett.* **2009**, *30*, 490.
[27] B. S. Ong, C. Li, Y. Li, Y. Wu, R. Loutfy, *J. Am. Chem. Soc.* **2007**, *129*, 2750.
[28] H. Li, J. Wang, H. Liu, C. Yang, H. Xu, X. Li, H. Cui, *Vacuum* **2004**, *77*, 57.
[29] H. K. Kim, K. K. Kim, S. J. Park, T. Y. Seong, I. Adesida, *J. Appl. Phys.* **2003**, *94*, 4225.
[30] A. Yakimov, S. R. Forrest, *Appl. Phys. Lett.* **2002**, *80*, 1667.
[31] A. Kumar, S. Sista, Y. Yang, *J. Appl. Phys.* **2009**, *105*, 094512.
[32] N. N. Greenwood, A. Earnshaw, *Chemistry of the Elements*, 2nd ed., **1997**, Butterworth-Heinemann, Oxford, UK.